1-1-2005

C and C+ in the Venusian Thermosphere/ Ionosphere

Jane L. Fox
Wright State University - Main Campus, jane.fox@wright.edu

L. J. Paxton

C and C^+ in the Venusian thermosphere/ionosphere

J. L. Fox
Department of Physics, Wright State University, Dayton, Ohio, USA

L. J. Paxton
Johns Hopkins University Applied Physics Laboratory, Laurel, Maryland, USA

Received 28 September 2004; revised 5 November 2004; accepted 16 November 2004; published 20 January 2005.

[1] We have constructed standard low and high solar activity models of the Venus thermosphere, which take into account revised rate coefficients for production and loss processes for C and C^+, high-resolution cross sections for photodissociation of CO, and recent solar fluxes from the Solar 2000 v1.24 and v2.22 models of *Tobiska* [2004]. Among the most important changes is the inclusion of the branching ratio for the channel of dissociative recombination of CO_2^+ that produces C + O_2, which has been measured recently by *Seiersen et al.* [2003]. We find that unlike Mars, where the production of C is dominated by dissociative recombination of CO_2^+, photodissociation of CO is the most important source of C in the Venus thermosphere, as previous models have shown. The loss of C is dominated by reaction with O_2 for molecular oxygen mixing ratios greater than 1×10^{-4}. We also construct here a model that is appropriate to the first year of the Pioneer Venus mission, when the solar activity was moderately high. We vary the O_2 mixing ratio at 90 km from 1×10^{-4} to 1×10^{-2}, and we predict the resulting C density profiles. By comparing these profiles to that derived from the Pioneer Venus Orbiter Ultraviolet Spectrometer limb profiles of the 1561 and 1657 Å resonance lines, we derive a "best fit" value of the O_2 abundance, which is determined to be slightly larger than 3×10^{-4}. We construct model density profiles of C^+ for four values of the the rate coefficient for the charge transfer reaction $O^+ + C \rightarrow C^+ + O$ from 1×10^{-11} to 3×10^{-10} cm^3 s^{-1}. We then compare the moderately high solar activity model C^+ profiles for a solar zenith angle of 25° to that obtained by the Pioneer Venus Orbiter Ion Mass Spectrometer for orbit 200, for which the value of $F_{10.7} \sim 200$. We find that the "best fit" rate coefficient for the charge transfer reaction is in the range $(0.9–1.3) \times 10^{-10}$ cm^3 s^{-1}.

Citation: Fox, J. L., and L. J. Paxton (2005), C and C^+ in the Venusian thermosphere/ionosphere, *J. Geophys. Res.*, *110*, A01311, doi:10.1029/2004JA010813.

1. Introduction

[2] The resonance multiplets of atomic carbon at 1561 Å ($^3D_J^o \rightarrow {}^3P_J$) and 1657 Å ($^3P_J^o \rightarrow {}^3P_J$) were first identified by *Rottman and Moos* [1973] in a spectrum of the Venus dayglow obtained by a rocket-borne far ultraviolet spectrometer. Intensities of ~2.4 and ~4.0 kR for the 1561 and 1657 Å emissions, respectively, were reported. The 1657 Å emission in the Venus dayglow was also detected by the ultraviolet spectrophotometers on the Mariner 10 flyby spacecraft, and a limb intensity of 30 kR was reported [*Broadfoot et al.*, 1974]. Spectra recorded by the Pioneer Venus (PV) Orbiter Ultraviolet Spectrometer (OUVS) also exhibited features at 1561 and 1657 Å [e.g., *Stewart et al.*, 1979; *Paxton*, 1983, 1985].

[3] The potential mechanisms for production of atomic carbon in the ground and excited states are photodissociation and electron-impact dissociation of CO_2 and CO, photodissociative ionization and electron-impact dissociative ionization of CO, and dissociative recombination of CO^+ and CO_2^+. Excited states of atomic carbon may also be produced by electron-impact excitation of ambient C; excited states that are connected to the ground state by dipole allowed transitions may also be produced by resonance scattering of solar radiation.

[4] For the expected range of mixing ratios of O_2 in the Venus thermosphere, loss of C is dominated by the reaction with O_2:

$$\text{(R11)} \qquad C + O_2 \rightarrow CO + O.$$

The rate coefficient for this reaction has been measured recently by *Chastaing et al.* [2000] and a value of $4.90 \times 10^{-11}(T_n/300)^{-0.32}$ cm^3 s^{-1} has been reported. The mixing ratio of O_2 in the Venus thermosphere has not, however, been measured. The mass spectrometers on the Pioneer Venus orbiter and bus could not distinguish between O and O_2 because the 32 amu mass peak was formed by

0148-0227/05/2004JA010813

recombination of O on the ion source surface [e.g., *Niemann et al.*, 1980]. Photochemical models of the Venus mesosphere have placed the mixing ratios of O_2 near 100 km as 2×10^{-3} [*Krasnopolsky and Parshev*, 1981] and 1×10^{-3} [*Yung and DeMore*, 1982].

[5] *Fox and Dalgarno* [1981] constructed a pre-Pioneer Venus model of the Venus dayglow. The predicted intensities of 78 and 39 R for the CI 1657 and 1561 Å emissions, respectively, were due solely to electron impact dissociative excitation and photodissociative excitation of CO_2. These mechanisms could not account for the intensities measured by Mariner 10 [*Broadfoot et al.*, 1974]. *Fox* [1982] and *Krasnopolsky* [1983] computed the atomic carbon densities in the Venusian thermosphere and showed that photodissociation of CO was the most important source of C. *Krasnopolsky* [1983] predicted an atomic carbon density profile that peaked near 140 km, with a value of about 1×10^7 cm^{-3} at high solar activity. The high solar activity model of *Fox* [1982] exhibited peak C densities that ranged from 5×10^6 to 3×10^7 cm^{-3} as the O_2 mixing ratio varied from 3×10^{-3} to 1×10^{-4}.

[6] All of the previous investigations suggested that resonance scattering of sunlight by atomic carbon was the most important source of the atomic carbon emission multiplets at 1561 and 1657 Å. Furthermore, *Fox* [1982] showed that photoionization of ambient C and photodissociative ionization of CO were the most important sources of C^+ at high altitudes and that these sources could explain the measured C^+ densities if the O_2 mixing ratio were $\sim 1 \times 10^{-4}$.

[7] In his analysis of the 1561 and 1657 Å emissions measured by the PV OUVS, *Paxton* [1985] derived a C density profile that peaked near 150 km, with a value of about 5×10^6 cm^{-3}, and that was characterized by a density of about 1.2×10^6 cm^{-3} near 250 km. The latter value is more important in determining the density of C because resonance scattering is most important at high altitudes. The "best fit" atomic carbon profile of Paxton corresponded to a thermospheric O_2 mixing ratio of $\sim 3 \times 10^{-3}$.

[8] Since these models were constructed, *Fox and Black* [1989] showed that because the photodissociation of CO longward of the ionization threshold at 885 Å proceeds mainly by line excitation into predissociating states, high-resolution cross sections must be constructed to determine the photodissociation rates. The use of high-resolution cross sections was shown to result in photodissociation rates that were about half of those obtained using low-resolution cross sections. We employ here the high-resolution photodissociation cross sections computed by Fox and Black averaged over 1 Å intervals in the range from threshold at 1118 Å to 885 Å, and low-resolution cross sections below 885 Å [*Cook et al.*, 1965]. For photoionization of C by photons with wavelengths less than 300 Å, we adopt the theoretical cross sections of *Verner and Yakovlev* [1995].

[9] Usually, dissociative recombination of CO_2^+ has been assumed to proceed via the channel

$$\text{(R2a)} \qquad CO_2^+ + e \rightarrow CO + O + 8.3\text{eV}.$$

Because of the significant rearrangement of bonds that must take place, the branching ratio for the channel

$$\text{(R2b)} \qquad CO_2^+ + e \rightarrow C + O_2 + 2.3\text{eV}$$

has been assumed to be negligible. The channel that forms a CO_2 molecule

$$\text{(R2c)} \qquad CO_2^+ + e \rightarrow CO_2 + 13.76\text{eV}$$

is not allowed at low pressures by conservation of energy and momentum unless a photon is emitted in the process, although at high pressures reaction (R2c) could proceed by three-body recombination. Such high pressures are, however, larger than those in the Venus thermosphere.

[10] *Seiersen et al.* [2003] have recently carried out measurements of the rate coefficient and products of dissociative recombination of CO_2^+ with the ion storage ring ASTRID and have reported a rate coefficient for reaction (R2) of $6.5 \times 10^{-7}(300/T_e)^{0.8}$ cm^3 s^{-1}. This value is larger at thermal energies than those measured in the Flowing Afterglow Langmuir Probe (FALP) experiments of 3.1×10^{-7} cm^3 s^{-1} reported by *Geoghegan et al.* [1991] and 3.5×10^{-7} cm^3 s^{-1} reported by *Gougousi et al.* [1997]. We adopted the latter rate coefficient with the theoretical temperature dependence of $(300/T_e)^{0.5}$ in most of our recent models of the Martian and Venusian ionospheres [e.g., *Fox and Sung*, 2001; *Fox and Bakalian*, 2001; *Fox*, 2003; *Fox*, 2004a]. *Seiersen et al.* reported branching ratios of $0.87 \pm .04$, 0.09 ± 0.03 and 0.04 ± 0.03 for the channels (R2a), (R2b), and (R2c), respectively. This is the first reported detection of channel (R2b) in measurements of dissociative recombination of CO_2^+. Since the channel (R2c) is not expected, in our recent study of thermal and nonthermal C densities in the Martian atmosphere, we adopted slightly different branching ratios for channels (R2a), (R2b), and (R2c) of 0.907, 0.093, and 0.0, respectively. We showed that dissociative recombination of CO_2^+ is the most important source of C in the Martian thermosphere [*Fox*, 2004b].

[11] We compute here the C and C^+ density profiles for standard low and high solar activity models of the Venus thermosphere/ionosphere. In our standard models we have adopted the 76200 spectra for low solar activity and the 79050 spectra for high solar activity for both the S2K v1.24 and S2K v2.22 solar flux models of *Tobiska* [2004] (K. Tobiska, private communication, 2003, 2004). The standard models are characterized by solar zenith angles (SZA) of 60° and an average heliocentric distance of 0.723 AU. We have here adopted the slightly modified branching ratios for reactions (R2a) and (R2b) that were discussed above for Mars. We chose the rate coefficient for CO_2^+ dissociative recombination measured by *Seiersen et al.* [2003] to be consistent with the measured branching ratios, which were based on that rate coefficient.

[12] The standard models are characterized by a mixing ratio of O_2 of 1×10^{-3}. The rate coefficient for the charge transfer reaction of O^+ with C:

$$\text{(R22)} \qquad O^+ + C \rightarrow O + C^+,$$

Table 1. Reactions Involving C and C^+

Number	Reaction	Rate Coefficient, $cm^3\ s^{-1}$	Reference
R1	$CO^+ + e \rightarrow C + O$	$1.8 \times 10^{-7}(T_e/300)^{-0.5}$	*Rosén et al.* [1998]
R2a	$CO_2^+ + e \rightarrow CO + O$	$5.90 \times 10^{-7}(T_e/300)^{-0.8}$	*Seiersen et al.* [2003]
R2b	$CO_2^+ + e \rightarrow C + O_2$	$6.05 \times 10^{-8}(T_e/300)^{-0.8}$	*Seiersen et al.* [2003]
R3	$N^+ + CO \rightarrow NO^+ + C$	$6.16 \times 10^{-11}(T_i/300)^{-0.4}$	*Anicich* [1993][a] *Miller et al.* [1984][b]
R4	$N^+ + CO \rightarrow C^+ + NO$	$5.6 \times 10^{-12}(T_i/300)^{-0.5}$	*Anicich* [1993] *Miller et al.* [1984]
R5	$C^+ + NO \rightarrow NO^+ + C$	$7.5 \times 10^{-10}(T_i/300)^{-0.2}$	*Anicich* [1993] *Miller et al.* [1984]
R6	$CO^+ + N \rightarrow NO^+ + C$	8.2×10^{-11}	*Scott et al.* [1998]
R7	$O^{++} + CO_2 \rightarrow C + \text{products}$	5×10^{-10}	estimate, see text
R8	$O^{++} + CO_2 \rightarrow C^+ + \text{products}$	5×10^{-10}	estimate, see text
R9	$O^{++} + CO \rightarrow C + \text{products}$	8×10^{-10}	estimate, see text
R10	$O^{++} + CO \rightarrow C^+ + \text{products}$	8×10^{-10}	estimate, see text
R11	$C + O_2 \rightarrow CO + O$	$4.9 \times 10^{-11}(T_n/300)^{-0.32}$	*Chastaing et al.* [2000]
R12	$C + NO \rightarrow CN + O$	$7.5 \times 10^{-11}(T_n/300)^{-0.16}$	*Chastaing et al.* [2000]
R13	$C + NO \rightarrow CO + N$	$7.5 \times 10^{-11}(T_n/300)^{-0.16}$	*Chastaing et al.* [2000]
R14	$C + CO_2 \rightarrow CO + CO$	$7.62 \times 10^{-14}(T_n/300)^{0.5}\ \exp(-3480/T_n)$	estimate, *McElroy and McConnell* [1971]
R15	$He^+ + CO \rightarrow C^+ + O + He$	1.6×10^{-9}	*Anicich* [1993]
R16	$He^+ + C \rightarrow C^+ + He$	$6.3 \times 10^{-15}(T_i/300)^{0.75}$	*Kimura et al.* [1993]
R17	$He^+ + CO_2 \rightarrow C^+ + O_2$	2×10^{-11}	*Anicich* [1993]
R18	$O_2^+ + C \rightarrow C^+ + O_2$	5×10^{-11}	estimate,
R19	$O_2^+ + C \rightarrow CO^+ + O$	5×10^{-11}	*Prasad and Huntress* [1980]
R20	$N_2^+ + C \rightarrow N_2 + C^+$	1.1×10^{-10}	UMIST [1999][c]
R21	$CO^+ + C \rightarrow CO + C^+$	5.2×10^{-11}	UMIST [1999]
R22	$O^+ + C \rightarrow C^+ + O$	see text	see text
R23	$C^+ + O_2 \rightarrow O + CO^+$	3.48×10^{-10}	*Anicich* [1993]
R24	$C^+ + O_2 \rightarrow O^+ + CO$	5.22×10^{-10}	*Anicich* [1993]
R25	$C^+ + CO_2 \rightarrow CO^+ + CO$	1.1×10^{-9}	*Fahey et al.* [1981]
R26	$C^+ + NO \rightarrow NO^+ + C$	$7.5 \times 10^{-10}(T_i/300)^{-0.2}$	*Anicich* [1993] *Miller et al.* [1984]
R27	$C^+ + H_2 \rightarrow CH^+ + H$	$7.4 \times 10^{-10}\exp(-4538/T_i)$	*Hierl et al.* [1997]

[a]Where the compilation of *Anicich* [1993] is referenced, the rate coefficient is the average of two or more measured values.
[b]Where the second reference is *Miller et al.* [1984] the temperature dependence has been taken from that reference.
[c]Where the UMIST [1999] compilation is referenced, the rate coefficient is the average of two or more calculated or measured values [*Le Teuff et al.*, 2000].

has not been measured. It has been assigned a value of 1×10^{-10} $cm^3\ s^{-1}$ in the standard models. We vary the value of k_{22} and determine the effect of different values of the rate coefficient on the predicted C^+ and C density profiles.

[13] *Fox and Sung* [2001] constructed low and high solar activity models of the Venus thermosphere/ionosphere based on the SC21REFW and F79050 solar fluxes, respectively, of H. E. Hinteregger (private communication, 1980) [cf. *Hinteregger et al.*, 1981; *Torr et al.*, 1979]. A comparison of the predicted high solar activity C profiles to those of *Paxton* [1985] and the predicted C^+ profiles to those presented by *Taylor et al.* [1980] for PV orbit 185 indicated that the O_2 abundance adopted in that model, 3×10^{-3}, was too high by a factor of ~3, and the rate coefficient k_{22} was less than 1×10^{-10} $cm^3\ s^{-1}$. The F79050 photon fluxes adopted in that model, however, were peak solar activity values, which were characterized by an $F_{10.7}$ of 238, and were larger than those appropriate to the first year of the PV mission, which began in 1978 December, when the periapsis of the PV spacecraft was in the range 140–160 km in the Venus thermosphere.

[14] In order to approximate the moderately high solar activity conditions that characterize the first year of the PV mission, we have constructed a model in which we adopted solar fluxes that are significantly less than those of the 79050 spectra. *Paxton* [1985] derived a C density profile from measurements made during the first year of the PV OUVS. The data set consisted of 5–15 limb scans of emission rates for each of five orbits at 1561 Å and nine orbits at 1657 Å. The signal at both wavelengths is contaminated by the CO fourth positive bands, and Paxton took this effect into account.

[15] For the purpose of comparing the computed C and C^+ density profiles with those measured on the PV spacecraft, we construct five models in which we adopted O_2 mixing ratios of 1×10^{-4}, 3×10^{-4}, 1×10^{-3}, 3×10^{-3}, and 1×10^{-2}. For each of the five models, we test the effects of assuming values for k_{22} of 1×10^{-11}, 3×10^{-11}, 1×10^{-10}, and 3×10^{-10} $cm^3\ s^{-1}$. We derive the value of the O_2 mixing ratio that best fits the C profile inferred by *Paxton* [1985]. We compare the computed C^+ density profiles with those measured by the PV Orbiter Ion Mass Spectrometer (OIMS) on Orbit 200 [cf. *Fox and Kliore*, 1997]. The C^+ density profiles from this orbit are typical of those recorded during the first year of the PV mission. We then derive the value of k_{22} that provides a best fit to the measured C^+ density profile.

2. Models

2.1. Neutral Densities

[16] We have constructed standard low and high solar activity models that are similar to those of our recent investigation [*Fox and Sung*, 2001], to which the reader is referred for details. The background neutral models contain twelve species, CO_2, Ar, N_2, O, CO, O_2, He, H, H_2, C, N, and NO. We compute densities of 14 ions (CO_2^+, N_2^+, Ar^+, $O^+(^4S)$, $O^+(^2D)$, $O^+(^2P)$, CO^+, C^+, N^+, O_2^+, NO^+, O^{++}, He^+, and H^+) and nine minor neutral species (NO, $N(^4S)$, $N(^2D)$, $N(^2P)$, C, $O(^1S)$, $O(^1D)$, H, and H_2). The thermospheres of Mars and Venus both consist mostly of CO_2 at low altitudes, with a small admixture of N_2 of 2–4%. The photolysis products of CO_2 and N_2: O, O_2, CO, N, and C, are also present; O becomes the

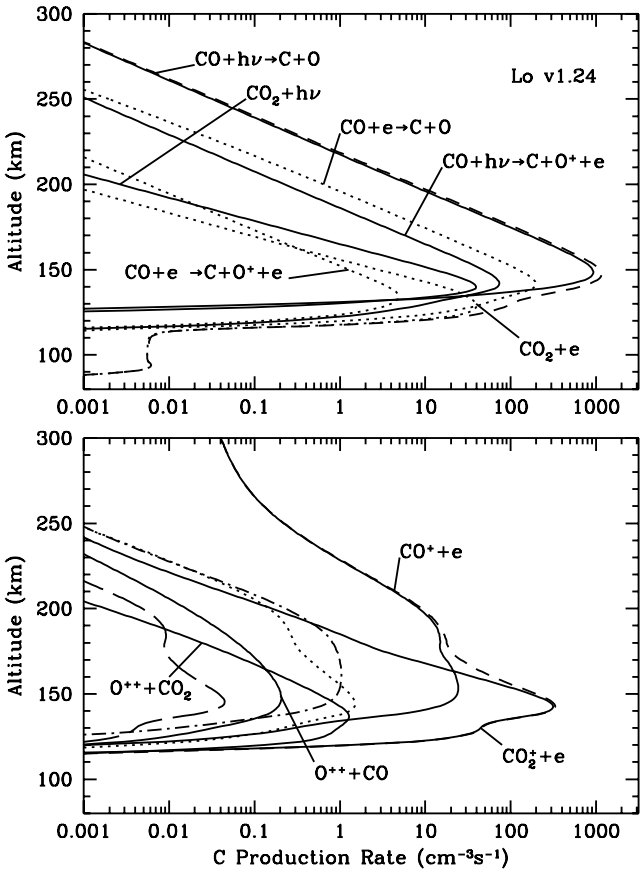

Figure 1. Computed production rate profiles for atomic carbon in the Venus thermosphere for the low solar activity model. "Lo v1.24" refers to the solar fluxes adopted: the 76200 S2K v1.24 spectrum of *Tobiska* [2004]. (top) The production rates due to the interaction of photons (solid curves) and photoelectrons (dotted curves) with CO_2 and CO. The total production rate is given by the dashed curve. (bottom) The production rate profiles of C in chemical reactions. The solid curves are labeled. The dotted curve represents the source due to the reaction of $N^+ + CO$ (reaction (R4)), the dot-dashed curve is the production profile due to the reaction of $CO^+ + N$ (reaction (R6)), and the long dashed curve is that due to the reaction of $C^+ + NO$ (reaction (R5)). The short dashed curve represents the total production rate.

dominant constituent of the thermospheres at high altitudes on both planets.

[17] The rate coefficients adopted here, other than that for the CO_2^+ dissociative recombination reaction, are largely the same as those compiled by *Fox and Sung* [2001], as updated by *Fox* [2003, 2004a]. The reactions involving C and C^+, their rate coefficients, and references are presented in Table 1. A few of the reactions merit discussion. The rate coefficients for the reactions involving O^{++} are the same as those adopted by *Fox and Victor* [1981]. These highly exothermic charge transfer reactions are assumed to produce fragmentation. A fraction 0.25 of the reactions of O^{++} with CO_2 is arbitrarily assumed to produce neutral C and a fraction 0.25 is assumed to produce C^+. For the reaction of O^{++} with CO, the total rate coefficient is assumed to be the same as that for the isoelectronic molecule N_2 [*Howorka et al.*, 1979]. Half of the reactions are assumed to produce neutral C and half C^+. Only upper limits have been measured for the reaction of C with CO_2. *Husain and Young* [1975] report an upper limit of 1×10^{-15} cm^3 s^{-1} at 300 K. Here we adopt the value estimated by *McElroy and McConnell* [1971], which is about 10^{-18} cm^3 s^{-1} at 300 K. The reaction of O_2^+ with C is assumed to proceed with a rate coefficient of 1×10^{-10} cm^3 s^{-1}, as estimated by *Prasad and Huntress* [1980], with half the reactions producing C^+ and half producing CO^+. As is evident, many of the rate coefficients for the reactions involving C and C^+ are estimates, which leads to some uncertainties in the modeled C and C^+ densities. The most important loss process for C^+ is the reaction with CO_2, which has been measured to proceed with a nearly gas kinetic rate coefficient of 1.1×10^{-9} cm^3 s^{-1} by *Fahey et al.* [1981].

[18] There are important differences between the thermospheres/ionospheres of Mars and Venus that relate to the abundance of atomic carbon. First, the mixing ratios of O are much larger in the thermosphere of Venus than in that of Mars. For example, at low solar activity, the

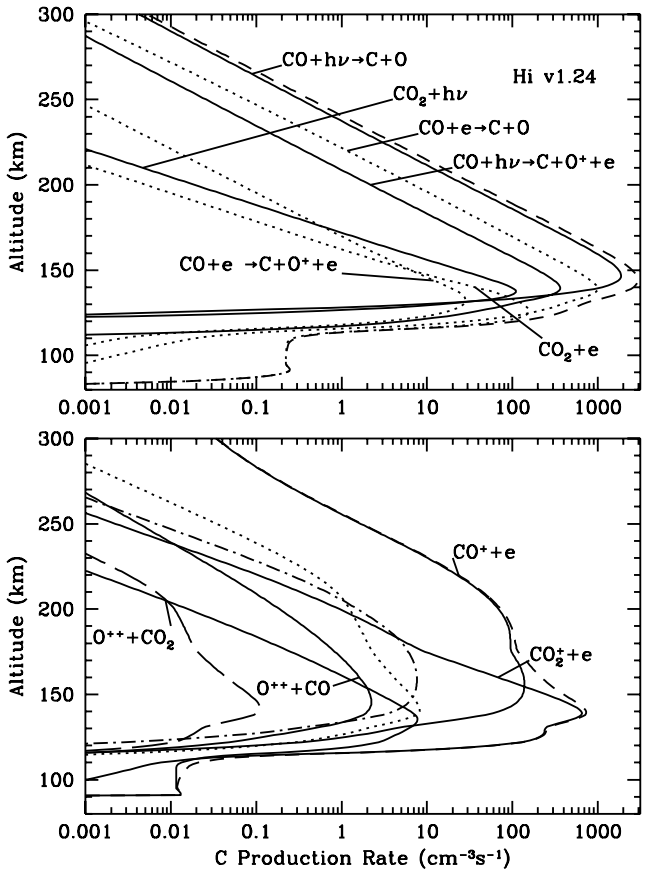

Figure 2. Computed production rate profiles for atomic carbon in the Venus thermosphere for the high solar activity model. "Hi v1.24" refers to the solar fluxes used in the model: the 79050 S2K v1.24 spectrum of *Tobiska* [2004] (see text). (top) The production rate profiles due to photon and photoelectron impact, and (bottom) the production rate profiles due to chemical reactions. The different curves represent the various chemical reactions as in Figure 1.

Table 2. Column Production Rates of C Atoms Due to Various Sources for the Standard Low and High Solar Activity S2K v1.24 and v2.22 Models (10^6 cm^{-2} s^{-1})

	S2K v1.24		S2K v.22	
Mechanism	Low Solar Activity	High Solar Activity	Low Solar Activity	High Solar Activity
$CO + h\nu \rightarrow C + O$	1.97(3)[a]	4.5(3)	1.04(3)	2.6(3)
$CO_2^+ + e \rightarrow C + O_2$	5.2(2)	1.30(3)	2.6(2)	5.3(2)
$CO + e \rightarrow C + O + e$	4.3(2)	2.3(3)	3.1(2)	1.20(3)
$CO + h\nu \rightarrow C + O^+ + e$	1.50(2)	8.0(2)	1.17(2)	4.4(2)
$CO^+ + e \rightarrow C + O$	1.18(2)	8.0(2)	5.4(1)	3.6(2)
CO_2+ e → C* + e + products	6.7(1)	2.6(2)	3.7(1)	1.00(2)
CO_2+ hν → C* + products	5.3(1)	1.51(2)	5.1(1)	1.16(2)
$CO + e \rightarrow C + O^+ + 2e$	9.7(0)	5.9(1)	5.2(0)	2.3(1)
$CO^+ + N \rightarrow NO^+ + C$	5.0(0)	3.7(1)	1.86(0)	1.41(1)
$N^+ + CO \rightarrow NO^+ + C$	4.8(0)	3.0(1)	3.2(0)	1.67(1)
$O^{++} + CO_2 \rightarrow C + O + 2O^+$	3.2(0)	1.88(1)	2.7(0)	1.13(1)
$O^{++} + CO \rightarrow C + 2O^+$	7.9(−1)	8.7(0)	8.4(−1)	6.2(0)
$C^+ + NO \rightarrow NO^+ + C$	1.27(−1)	3.8(−1)	5.6(−2)	1.64(−1)
Total	3.3(3)	1.03(4)	1.88(3)	5.4(3)

[a]Read as 1.97×10^3.

mixing ratio of O at the ion peak on our Mars model is ∼0.02 [e.g., *Fox and Dalgarno*, 1979; *Fox*, 2004b]. According to the VTS3 model of the Venus thermosphere [*Hedin et al.*, 1983], which is based on in situ measurements of the PV Orbiter Neutral Mass Spectrometer (ONMS) [e.g., *Niemann et al.*, 1980], and normalized to the PV Orbiter Ion Drag data [e.g., *Keating et al.*, 1980; *Keating*, 1985], the mixing ratio of O at the low solar activity ion peak is ∼0.10. At high solar activity, the VTS3 model O mixing ratio at the ion peak of Venus is ∼0.20. Although there are no in situ data about the O mixing ratio at high solar activity on Mars, the Mars Thermospheric General Circulation Model (MTGCM) of *Bougher et al.* [1999, 2000] shows little variation in the O mixing ratio with solar activity. Bougher et al. suggest that on Mars, the O abundance variations over a solar cycle may be limited by dynamical processes, including turbulence and convection. Because CO_2^+ is transformed to O_2^+ in the reaction with O:

$$CO_2^+ + O \rightarrow O_2^+ + CO, \quad (1)$$

the larger abundance of O implies that a larger fraction of the CO_2^+ produced will be transformed to O_2^+ in the Venus ionosphere than in the Martian ionosphere, thus diminishing the importance of the dissociative recombination of CO_2^+ as a source of C.

[19] In addition, the CO mixing ratios in the Venus thermosphere are larger than those on Mars. The mixing ratio of CO measured by the Viking mass spectrometer [e.g., *Nier et al.*, 1976; *Nier and McElroy*, 1976, 1977] is about 0.01 at the ion peak on Mars. There is no information about the CO mixing ratio in the atmosphere of Mars at high solar activity. For the MTGCM model that we employed in our recent Mars model [*Fox*, 2004b], the mixing ratio of CO at high solar activity is about 0.03 at the ion peak. For the low solar activity Venus thermosphere, we have adopted the VTS3 model for $F_{10.7} = 80$. This model exhibits a CO abundance near the ion peak of about 0.07; at high solar activity, for $F_{10.7} = 200$, the mixing ratio of CO near the ion peak is about 0.12. Since the mixing ratios of CO are larger on Venus, processes associated with the dissociation and dissociative ionization of CO, including production of C and C^+, should be more important on Venus than on Mars.

[20] We have included here K-shell ionization of O, C, and N, and the subsequent decay by emission of an Auger electron. The cross sections for K-shell ionization of atoms were adopted from *Verner and Yakovlev* [1995]. For molecules, the K-shell ionization cross sections were assumed to be the sum of the cross sections for the constituent atoms. The energy range of the photoelectron spectrum is 0 to 600 eV in intervals of 1.0 eV, as in our most recent models [cf. *Fox*, 2004a, 2004b].

2.2. Solar Fluxes

[21] As mentioned above, for the standard low and high solar activity models, we have adopted the 76200 and 79050 solar fluxes, respectively, from the Solar 2000 (S2K) v1.24 and v2.22 models of *Tobiska* [2004] (K. Tobiska, private communication, 2003, 2004). The photon fluxes of the v1.24 models were normalized to the soft X-ray fluxes measured by the Student Nitric Oxide Explorer (SNOE) Solar X-ray Photometer [e.g., *Barth et al.*, 1999; *Bailey et al.*, 2000]. The S2K v2.22 models are normalized to the measurements of the Thermosphere Ionosphere Mesosphere Energetics and Dynamics mission (TIMED) Solar EUV Experiment instrument [e.g., *Woods et al.*, 2000]. The photon fluxes in the soft X-ray and EUV regions are significantly larger in the v1.24 solar flux models than those in the v2.22 models.

[22] In order to predict the C and C^+ density profiles appropriate to the first year of the PV mission, we have constructed a moderately high solar activity model. Because the v2.22 solar flux models are expected to be more accurate than the v1.24 models (K. Tobiska, private communication, 2004), we have adopted the S2K v2.22 99178 solar flux spectrum, which is characterized by an $F_{10.7}$ of ∼207.4 and an 81 day average $F_{10.7}$ of 166.3. Since Venus was on the opposite side of the Sun from the Earth for orbit 200, we average the lead and lag of Venus relative to Earth, and we obtain a similar $F_{10.7}$ of 197 and an 81 day average $F_{10.7}$ of 203. In order to compare the C^+ density profiles to those of orbit 200, we have adopted the solar zenith angle at periapsis of this orbit, which is ∼25°.

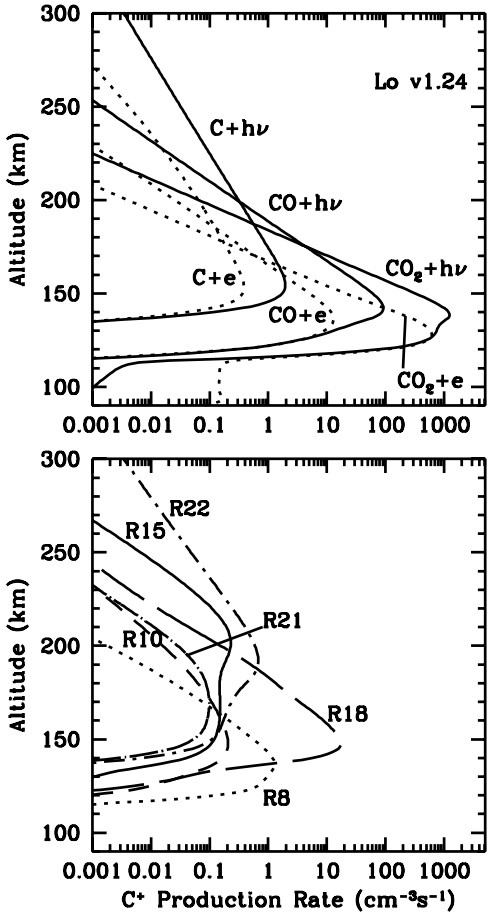

Figure 3. Computed production rate profiles for C^+ in the Venus ionosphere for the low solar activity model. "Lo v1.24" refers to the solar fluxes adopted: the 76200 S2K v1.24 spectrum of *Tobiska* [2004]. (top) The production rates due to the interaction of photons (solid curves) and by photoelectrons (dotted curves) with C, CO, and CO_2. The total production rate is given by the dashed curve. (bottom) The production rate profiles of C^+ in chemical reactions. The curves are labeled with the reaction numbers as shown in Table 1.

[23] In the versions of the solar spectra that we adopted, the photon fluxes are given as delta functions at the strong solar lines and at 1 Å intervals in the continuum from 18 to 2000 Å, for a total of 1811 wavelengths. Below 18 Å we have adopted the solar fluxes from *Ayres* [1997] (T. Ayres, private communication, 1996). These harder X ray solar fluxes are highly variable, but are absorbed at altitudes less than about 100 km, which is outside the region of interest in this model.

3. C and C^+ Production and Loss Processes

[24] The production rates of atomic carbon are shown in Figures 1 and 2 for the S2K v1.24 low and high solar activity models, respectively. The upper panels show the sources due to photon absorption and photoelectron impact on CO and CO_2. The total integrated column production rates of C due to various sources are presented in Table 2 for both the S2K v1.24 and v2.22 solar flux models. The production rates for the S2K v2.22 solar flux models are smaller than those for the v1.24 models by factors that are of the order of 2. The total production rates of C are in the ranges $(1.88-3.3) \times 10^9$ and $(0.54-1.03) \times 10^{10}$ cm^{-2} s^{-1} for the low and high solar activity models, respectively. The smaller column production rates in the stated range, both here and in the text that follows, are those computed using the S2K v2.22 solar fluxes, and the larger rates are those computed using the v1.24 solar fluxes. At both low and high solar activities, photodissociation of CO dominates the production of C above about 140 km; the altitudes of peak production are in the range 147–148 km. The column production rates of atomic carbon from photodissociation of CO are $(1-2) \times 10^9$ and $(2.6-4.5) \times 10^9$ cm^{-2} s^{-1}, for the low and high solar activity models, respectively.

[25] Electron-impact dissociation of CO, and photodissociative ionization of CO are also important sources of C; electron impact processes dominate the production of C below 130 km. We should note here that the production

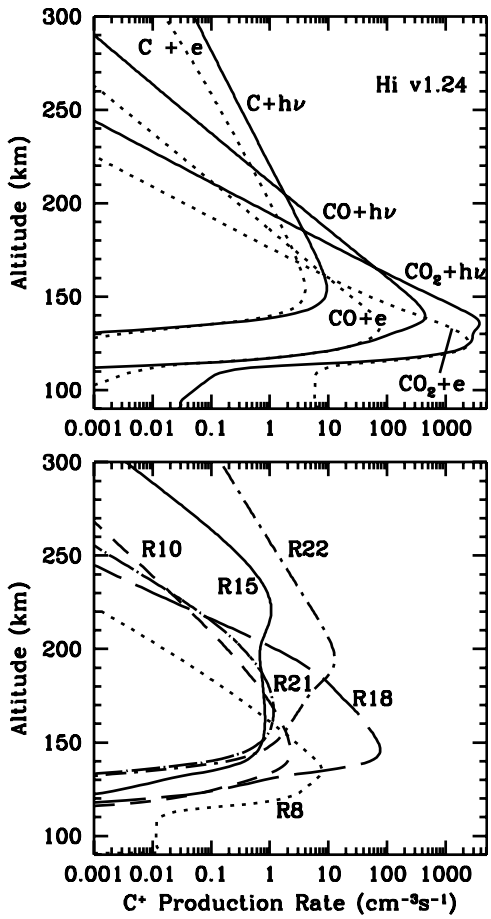

Figure 4. Computed production rate profiles for C^+ in the Venus ionosphere for the high solar activity model. "Hi v1.24" refers to the solar fluxes adopted: the 79050 S2K v1.24 spectrum of *Tobiska* [2004]. (top) The production rates due to the interaction of photons (solid curves) and by photoelectrons (dotted curves) with C, CO, and CO_2. (bottom) The production rate profiles of C^+ in chemical reactions. The curves are labeled with the reaction numbers as shown in Table 1.

Table 3. Column Production Rates of C^+ Ions Due to Various Sources for the Standard Low and High Solar Activity S2K v1.24 and 2.22 Models (10^6 cm^{-2} s^{-1})

	S2K v1.24		S2K v2.22	
Mechanism	Low Solar Activity	High Solar Activity	Low Solar Activity	High Solar Activity
CO_2+ h$\nu \rightarrow C^+$ + e + products	2.4(3)[a]	7.9(3)	1.63(3)	3.8(3)
CO_2+ e $\rightarrow C^+$ +2e + products	9.1(2)	3.6(3)	4.4(2))	1.32(3)
CO + h$\nu \rightarrow C^+$ + O + e	1.90(2)	1.00(3)	1.43(2)	5.8(2)
CO + e $\rightarrow C^+$ + O +2e	2.9(1)	1.74(2)	2.0(1)	8.4(1)
O_2^+ + C $\rightarrow C^+ + O_2$	3.7(1)	2.1(2)	1.72(1)	9.3(1)
O^+ + C $\rightarrow C^+$ + O	3.2(0)	6.1(1)	1.13(0)	2.2(1)
C + h$\nu \rightarrow C^+$ + e	7.0(0)	4.1(1)	2.0(0)	1.44(1)
O^{++} + $CO_2 \rightarrow C^+$ + products	3.2(0)	1.88(1)	2.7(0)	1.13(1)
C + e $\rightarrow C^+$ +2e	1.40(0)	1.83(1)	6.1(−1)	6.3(0)
He^+ + CO $\rightarrow C^+$ + O + He	1.39(0)	8.9(0)	9.5(−1)	5.0(0)
O^{++} + CO $\rightarrow C^+$ +2O	7.9(−1)	8.7(0)	8.4(−1)	6.2(0)
CO^+ + C $\rightarrow C^+$ + CO	4.5(−1)	5.2(0)	1.53(−1)	1.83(0)
N^+ + CO $\rightarrow C^+$ + NO	4.3(−1)	2.7(0)	3.0(−1)	1.52(0)
N_2^+ + C $\rightarrow C^+ + N_2$	1.09(−1)	7.2(−1)	3.9(−2)	2.6(−1)
He^+ + $CO_2 \rightarrow C^+$ + O + He	2.1(−2)	7.3(−2)	1.48(−2)	4.1(−2)
He^+ + C $\rightarrow C^+$ + He	4.0(−7)	1.03(−5)	1.45(−7)	2.9(−6)
Total	3.6(3)	1.30(4)	2.2(3)	5.8(3)

[a]Read as 2.4×10^3.

rates of C from electron-impact dissociation and photodissociation of CO_2 include only excited carbon, and the total production rate of atomic carbon from these sources may be larger.

[26] Atomic carbon is produced in several chemical reactions, as shown in Table 1. The computed production rate profiles for the chemical sources of atomic carbon are shown in the bottom panels of Figures 1 and 2 for the S2K v1.24 low and high solar activity models, respectively. Dissociative recombination of CO_2^+ clearly dominates the chemical production of C, with peak production rates occurring near 145–150 km. Table 2 shows that the column integrated production rates due to dissociative recombination of CO_2^+ are (2.6–5.2) $\times$ 10^8 and (0.53–1.30) $\times$ 10^9 cm^{-2} s^{-1}, at low and high solar activities, respectively. Although important, this mechanism only provides 10–16% of the total source of atomic carbon. At high altitudes, CO^+ dissociative recombination is more important than dissociative recombination of CO_2^+ but the integrated column production rates are less. Loss of C is dominated by the reaction with O_2 (reaction (R11)), with some contribution from reaction with NO (reactions (R12) and (R13)). The importance of the reactions with NO depends on the mixing ratio of O_2 in the models. For the standard models, in which the O_2 abundance is 1×10^{-3}, the altitude integrated loss rate due to reaction with NO is $\sim$10 times less than that for reaction with O_2. Thus we expect that for models in which the O_2 abundance is greater than $\sim 1 \times 10^{-4}$, reaction with O_2 should be the most important loss process.

[27] At very low altitudes of the high solar activity model, the most important production process for C is reaction of O^{++} with CO_2 (reaction (R8)). The O^{++} in this altitude range is produced by electron impact double ionization of O. As is well known, in this region of the Venus thermosphere, high-energy EUV and soft X-ray photons are absorbed. Ionization by these photons can produce Auger and other high-energy photoelectrons, which are capable of producing multiple excitations, dissociations, and ionizations before they are thermalized. As Table 2 shows, however, the column integrated rates of production of C and C^+ arising from reactions of O^{++} are small.

[28] Altitude profiles of the major sources of C^+ are presented in Figures 3 and 4 for the low and high solar activity S2K v1.24 models, respectively. The column integrated production rates for both the S2K v1.24 and v2.22 models are presented in Table 3. The major sources of C^+ near 140 km are photodissociative ionization and electron-impact dissociative ionization of CO_2, with column integrated production rates of (1.63–2.4) $\times$ 10^9 and (3.8–7.9) $\times$ 10^9 cm^{-3} s^{-1}, at low and high solar activities, respectively. Photodissociative ionization and electron-impact dissociative ionization of CO have fairly large column integrated production rates. These sources peak, however, at low altitudes. At high altitudes, the most important sources of C^+ are photoionization and electron-impact ionization of C, and the charge transfer reaction from O^+ to C (reaction (R22)).

[29] The computed density profiles of C and C^+ for the standard S2K v1.24 and v2.22 models for low and high solar activities, respectively, are presented in Figures 5 and 6, respectively. The density profiles for four values of the rate coefficient for the charge transfer reaction of O^+ to C, k_{22}, 1×10^{-11}, 3×10^{-11}, 1×10^{-10}, and 3×10^{-10} cm^3 s^{-1}, are shown for each solar flux model. The predicted carbon density profiles, which are overplotted for the four cases, show no visible dependence on the value assumed for k_{22} for the range of our calculations. The peak C densities are 1.34×10^6 and 7.7×10^5 cm^{-3} at low solar activity and are 4.2×10^6 and 2.4×10^6 cm^{-3} at high solar activity, for the S2K v1.24 and v2.22 models, respectively. At low solar activity, as the adopted value of k_{22} varies from 1×10^{-11} to 3×10^{-10} cm^3 s^{-1}, the predicted C^+ density peaks increase from 1.2×10^3 to 3.0×10^3 cm^{-3} for the v2.22 models and from 0.62×10^4 to 1.25×10^4 cm^{-3} for the v1.24 models. For the analogous high solar activity v2.22 and v1.24 and models, the C^+ peak density ranges are (0.45–1.06) $\times$ 10^4 and (1.1–4.2) $\times$ 10^4 cm^{-3}, respectively. Thus the C^+ densities increase by factors of 2–4 as the value of k_{22} is increased by a factor of 30. The

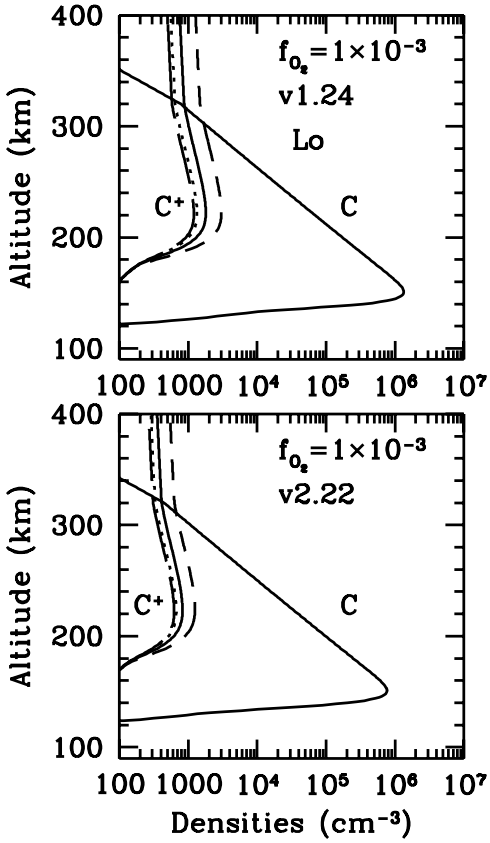

Figure 5. Altitude profiles of the densities of C and C^+ for the low solar activity models for an O_2 abundance of 1×10^{-3}. (top) The altitude profiles computed with the S2K v1.24 solar fluxes and (bottom) the results for the S2K v2.22 model [e.g., *Tobiska*, 2004]. The C^+ density profiles are given in each panel for four values of the rate coefficient, k_{22}, for the charge transfer reaction of O^+ with C. The long dashed curve shows the C^+ densities for $k_{22} = 1 \times 10^{-11}$, the dotted curve shows those for $k_{22} = 3 \times 10^{-11}$, the solid curve shows those for $k_{22} = 1 \times 10^{-10}$, and the short-dashed curve shows those for $k_{22} = 3 \times 10^{-10}$ cm^3 s^{-1}. The densities of C for each value of k_{22} are overplotted in each panel and clearly are not sensitive to the adopted value of k_{22}.

C^+ density profile that was measured by the PV OIMS for Orbit 185 [*Taylor et al.*, 1980], and which was compared to the models of *Fox* [1982] and *Fox and Sung* [2001], exhibits a peak C^+ density of about 8×10^3 cm^{-3}. We find that generally, the high solar activity C^+ densities for the S2K 2.22 solar fluxes are in better agreement with the measurements than are those for the S2K v1.24 models. Since the v2.22 solar fluxes are now considered to be more accurate than the v1.24 solar fluxes, this agreement is gratifying.

[30] In order to compare our predicted C and C^+ profiles to the C density profiles derived by *Paxton* [1985] and to the C^+ densities measured by the PV OIMS for orbit 200, we have constructed a moderately high solar activity model, using the 99178 S2K v2.22 solar fluxes, as describe above. We have constructed five models with O_2 mixing ratios of 1×10^{-4}, 3×10^{-4}, 1×10^{-3}, 3×10^{-3}, and 1×10^{-2}. The four panels of Figure 7 show the atomic carbon density profiles for O_2 abundances from 1×10^{-4} to 3×10^{-3}. In each panel the predicted C^+ density profiles for the four values of k_{22} are compared with the high-resolution C^+ profiles measured by the OIMS on orbit 200 (inbound) [cf. *Fox and Kliore*, 1997]. The oscillations in the C^+ OIMS measured densities are due to the spin of the spacecraft, the effects of which have not been accounted for. We can therefore derive from the data only a range of C^+ maxima, which appears to be $\sim(7-9) \times 10^3$ cm^{-3}. There also seems to be a vertical offset in the C^+ density data compared to the model. This may be due to errors in the neutral density profiles assumed. The neutral density models we have adopted are from the analytical VTS3 models, for which latitude, local time and $F_{10.7}$ can be specified, but which cannot be compared to any individual orbit. The relative neutral densities measured by the ONMS are more accurate than the absolute values, which have been normalized to the atmospheric drag data in the VTS3 model.

[31] For completeness, we should note that it is also possible that the low-altitude measured C^+ density profiles are too large. The density profiles of O_2^+ measured by the PV OIMS exhibit a peak in the range 160 to 180 km and are generally considered to be in error. Most of the models show an O_2^+ and total electron density peak near 140 km, as do the molecular ion densities measured by the RPA [e.g., *Knudsen*, 1992] and the total electron density profiles obtained by the Langmuir probe [e.g., *Brace et al.*, 1983]. The error could apply to the other ion densities in this

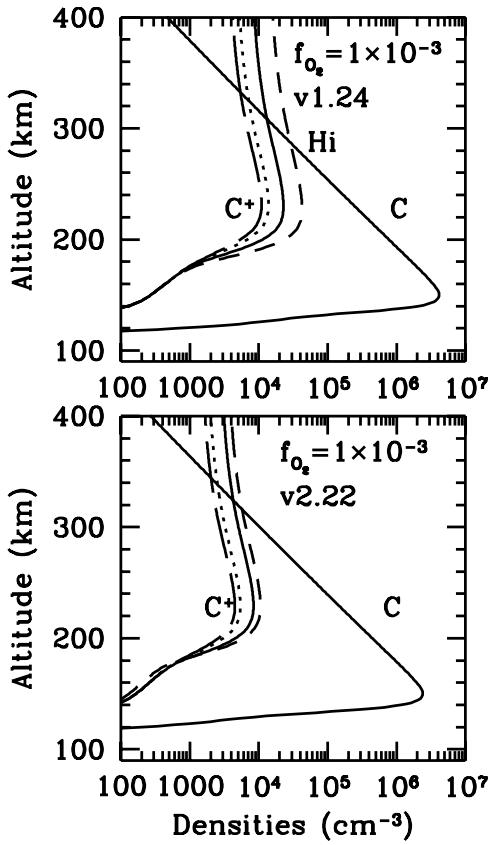

Figure 6. Same as for Figure 5, except for the high solar activity models.

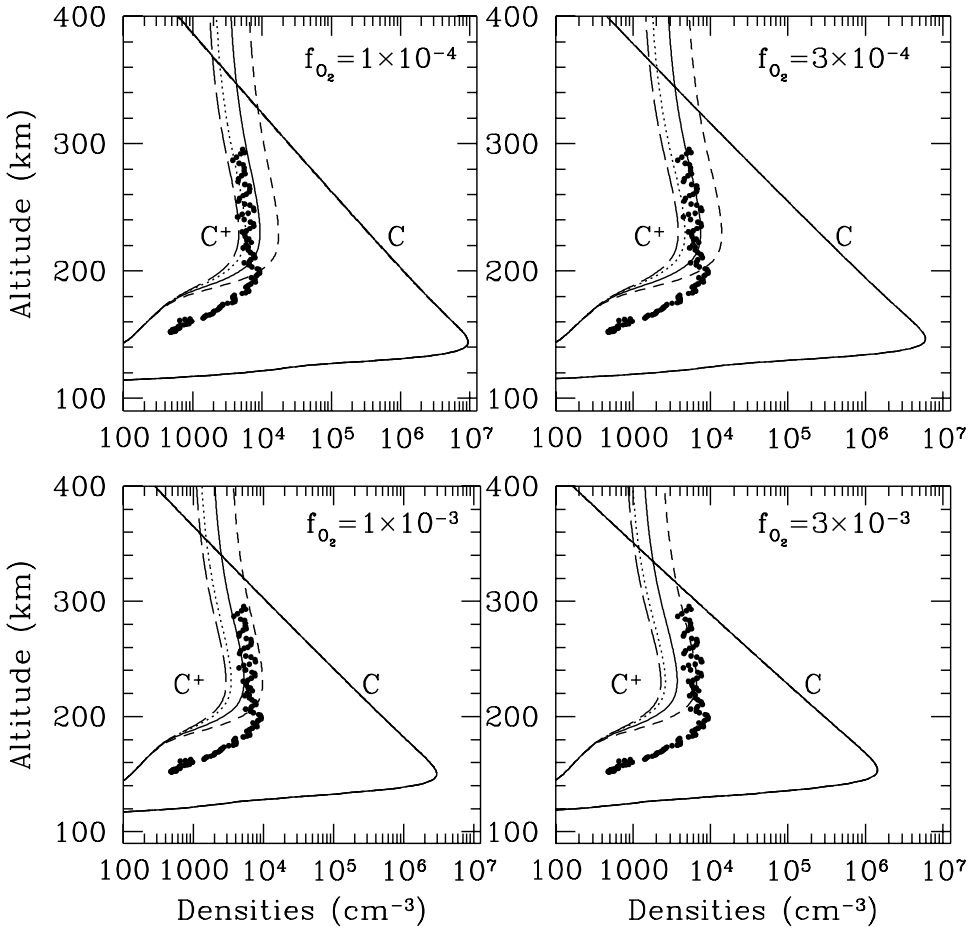

Figure 7. Altitude profiles of the densities of C and C^+ for the moderately high solar activity model, which is designed to apply to the first year of the Pioneer Venus mission (see text). Each panel is labeled with the assumed value of the mixing ratio of O_2 in the lower thermosphere. The models for O_2 abundances of 1×10^{-4}, 3×10^{-4}, 1×10^{-3}, and 3×10^{-3} are shown. The model for an O_2 abundance of 1×10^{-2} was computed but is not shown. The C^+ density profiles are given in each panel for four values of the rate coefficient, k_{22}. The long dashed curves show the C^+ densities for $k_{22} = 1 \times 10^{-11}$, the dotted curves are for $k_{22} = 3 \times 10^{-11}$, the solid curves are for $k_{22} = 1 \times 10^{-10}$, and the short-dashed curves are for $k_{22} = 3 \times 10^{-10}$ cm^3 s^{-1}. The C density profiles for each of these cases are overplotted and clearly do not vary with k_{22}.

region as well, although the atomic ion density profiles in general are not considered to be in significant error. If we assume that the measured lower-altitude C^+ densities are accurate, it is possible that the rate coefficient for the charge transfer reaction of O_2^+ with C (reaction (R18)), which is estimated in our model, is too small. It is unlikely that the loss rate of C^+, which in this region is mainly by reaction with CO_2 (reaction (R25)) is too large. We consider a vertical offset to be most likely, however, and we will therefore compare only the peak measured and model C^+ densities.

[32] The model atomic carbon density profiles derived by *Paxton* [1985] are shown in Figure 8. Atomic carbon density profiles could not be measured with the PV ONMS, since the mass peak at 12 amu arose primarily from fragmentation of CO [e.g., *Niemann et al.*, 1980]. The model that *Paxton* [1985] found to best fit the PV OUVS measured limb intensities of the 1561 and 1657 Å resonance lines was that which was characterized by an O_2 abundance of 3×10^{-3}. As mentioned previously, the peak C density of this profile near 150 km is $\sim 5 \times 10^6$ cm^{-3}, and the density at 250 km is $\sim 1.2 \times 10^6$ cm^{-3}. Models of the Venus thermosphere/ionosphere have undergone significant revisions in the last 20 years. Here we find that the best fit C profile is that for an O_2 mixing ratio of close to 3×10^{-4}. For this profile, the peak C density is $\sim 6 \times 10^6$ cm^{-3}, and the density at 250 km is $\sim 1.2 \times 10^6$ cm^{-3}, in good agreement with the density profile derived by *Paxton* [1985] from the PV OUVS intensities.

[33] In Figure 9, we plot the C^+ peak density versus k_{22} for the S2K v2.22 99178 moderately high solar activity model for five values of the O_2 mixing ratio. The horizontal dashed lines in the figures show the approximate range of peak C^+ densities at high solar activity. Table 4 shows the C peak and 250 km densities and the range of k_{22} derived from Figure 9 for the five models with O_2 mixing ratios from 1×10^{-4} to 1×10^{-2}. If we assume that the most likely O_2

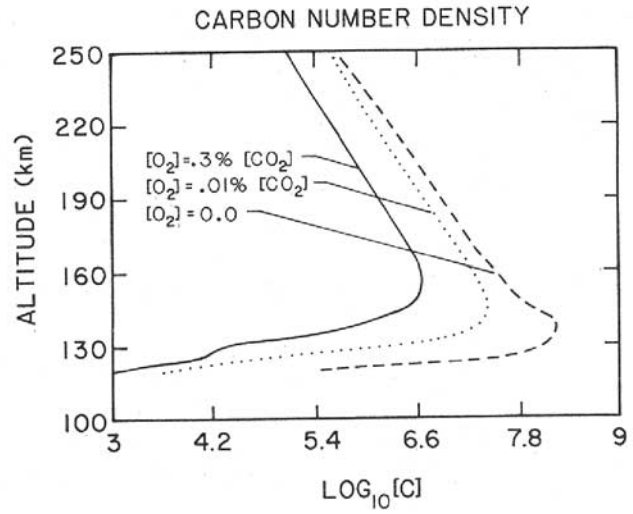

Figure 8. Altitude profiles of the densities of C derived by *Paxton* [1985] for various values of the O_2 mixing ratio. The solid profile was found to be a best fit to the PV OUVS 1561 and 1657 Å limb profiles.

mixing ratio is $\sim 3 \times 10^{-4}$, the best fit range of k_{22} is $\sim(0.9-1.3) \times 10^{-10}$ cm^3 s^{-1}.

4. Conclusions

[34] We have constructed standard low and high solar activity models of the Venus thermosphere/ionosphere, in which we include cross sections and rate coefficients for the processes involving production and loss of C and C^+ that have been revised since the studies of *Fox* [1982], *Krasnopolsky* [1983], and *Paxton* [1985]. In particular, we have included the revised cross sections for the photodissociation of CO [*Fox and Black*, 1989], the revised rate coefficient for the loss of C by reaction with O_2 (reaction (R11)) measured by *Chastaing et al.* [2000], and the rate coefficient for the production of C in dissociative recombination of CO_2^+ (reaction (R2b)) recently measured by *Seiersen et al.* [2003]. In the standard models, we have adopted the modern S2K v1.24 and S2K v2.22 solar flux models of *Tobiska* [2004] (K. Tobiska, private communication, 2003, 2004), an O_2 abundance of 1×10^{-3}, and a rate coefficient for charge transfer from O^+ to C of 1×10^{-10} cm^3 s^{-1}. We find that the predicted density profiles for the S2K v2.22 solar flux models fit the Pioneer Venus C and C^+ data better than do those of the S2K v1.24 models.

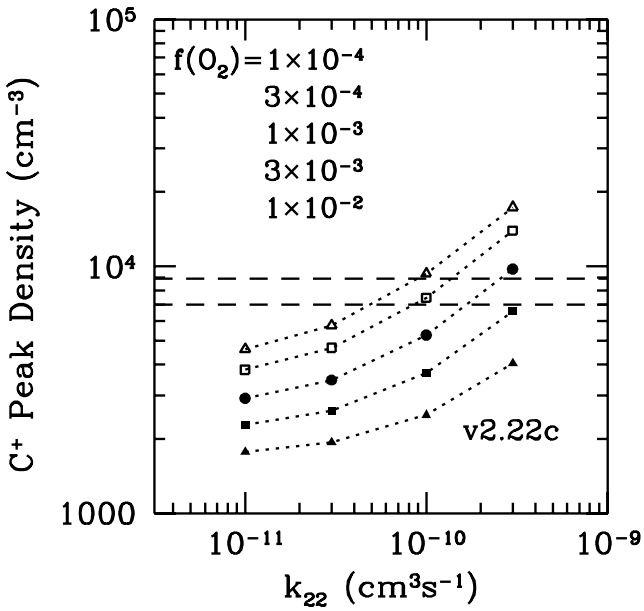

Figure 9. C^+ peak density versus the rate coefficient assumed for reaction (R22), k_{22}. The various curves are for different values of the mixing ratio of O_2 and are listed from top to bottom in the figure in the same order as the curves. The horizontal dashed lines delimit the range of the peak density derived from the C^+ density profile for Orbit 200 of the Pioneer Venus Spacecraft.

Table 4. C Densities at Peak and 250 km and k_{22} Values Corresponding to Various O_2 Mixing Ratios

Mixing Ratio of O_2	C Density (peak), cm^{-3}	C Density (250 km), cm^{-3}	k_{22}, cm^3 s^{-1}
1×10^{-4}	9.5×10^6	1.62×10^5	$(0.5-0.7) \times 10^{-10}$
3×10^{-4}	6.0×10^6	1.19×10^5	$(0.9-1.3) \times 10^{-10}$
1×10^{-3}	3.0×10^6	7.3×10^4	$(1.7-2.6) \times 10^{-10}$
3×10^{-3}	1.44×10^6	4.3×10^4	$\geq 3 \times 10^{-10}$
1×10^{-2}	5.8×10^5	2.3×10^4	N/A

[35] In a recent model of the Martian thermosphere, we showed that dissociative recombination of CO_2^+ is the most important source of thermal but not escaping C [*Fox*, 2004b]. By contrast, for Venus, the dominant source of C is photodissociation of CO, followed by dissociative recombination of CO_2^+. The difference can be easily understood as arising from quantitative differences between the thermospheres of Venus and Mars. First, the larger mixing ratio of O in the Venus thermosphere leads to a larger ratio of O_2^+ to CO_2^+, which limits the importance of dissociative recombination of CO_2^+. Second, the mixing ratio of CO is larger in the Venus thermosphere than in the thermosphere of Mars, so the C and C^+ sources due to interaction of CO with photons and photoelectrons are more important than those on Mars.

[36] By constructing a moderately high solar activity model of the Venus thermosphere/ionosphere and comparing the results to PV measurements of the C profile obtained during the first year of the mission, we have derived a "best fit" thermospheric mixing ratio of O_2 of $\sim 3 \times 10^{-4}$. Combining this with PV measured C^+ profiles, we have derived the "best fit" values for the rate coefficient for the charge transfer reaction of O^+ to C (reaction (R22)) and have predicted a value of $(0.9-1.3) \times 10^{-10}$ cm^3 s^{-1}.

[37] The data used here are from the early part of the PV mission. In the future we plan to extend our analysis to the entire PV OUVS database. This would give us the opportunity to examine the solar activity variability of the atomic carbon resonance features and the CO fourth positive bands. In addition to limb profiles, we will examine data from the illuminated disk that may provide insight into the photochemistry of C, O, and CO. An orbit by orbit analysis may be valuable, although in situ and remote sensing data are not

obtained simultaneously. We will incorporate into our model updated solar flux intensities and line shape data at the CI features and the revised production rates of the C multiplets and the CO fourth positive bands.

[38] **Acknowledgments.** This work has been supported by grants NAG5-12755 and MAG5-13313 from the National Aeronautics and Space Administration and by grant AST-9802007 from the National Science Foundation to Wright State University. The Solar2000 research grade irradiances are provided courtesy of W. Kent Tobiska and SpaceWx. These historical irradiances have been developed with funding from the NASA UARS, TIMED, and SOHO missions.

[39] Arthur Richmond thanks Alexander Dalgarno and another reviewer for their assistance in evaluating this paper.

References

Anicich, V. G. (1993), Evaluated bimolecular ion-molecule gas phase kinetics of positive ions for use in modeling planetary atmospheres, cometary comae, and interstellar clouds, *J. Chem. Phys. Ref. Data*, *22*, 1469–1569.

Ayres, T. (1997), Evolution of the solar ionizing flux, *J. Geophys. Res.*, *102*, 1641–1651.

Bailey, S. M., T. N. Woods, C. A. Barth, S. C. Solomon, L. R. Canfield, and R. Korde (2000), Measurements of the solar soft X-ray irradiance by the Student Nitric Oxide Explorer: First analysis and underflight calibrations, *J. Geophys. Res.*, *105*, 27,179–27,193.

Barth, C. A., S. C. Bailey, and S. C. Solomon (1999), Solar-terrestrial coupling: Solar soft X-rays and thermospheric nitric oxide, *Geophys. Res. Lett.*, *26*, 1251–1254.

Bougher, S. W., S. Engel, R. G. Roble, and B. Foster (1999), Comparative terrestrial planet thermospheres: 2. Solar cycle variation of global structure and winds at equinox, *J. Geophys. Res.*, *104*, 16,591–16,611.

Bougher, S. W., S. Engel, R. G. Roble, and B. Foster (2000), Comparative terrestrial planet thermospheres: 3. Solar cycle variation of global structure and winds at solstices, *J. Geophys. Res.*, *105*, 17,669–17,692.

Brace, L. H., H. A. Taylor, T. I. Gombosi, A. J. Kliore, W. C. Knudsen, and A. F. Nagy (1983), The ionosphere of Venus: Observations and their interpretations, in *Venus*, edited by D. M. Hunten et al., pp. 779–840, Univ. of Ariz. Press, Tucson.

Broadfoot, A. L., S. Kumar, M. J. S. Belton, and M. B. McElroy (1974), Ultraviolet observations of Venus from Mariner 10: Preliminary results, *Science*, *183*, 1315–1318.

Chastaing, D., S. D. Le Picard, and I. R. Sims (2000), Direct kinetic measurements on reactions of atomic carbon, C (^3P), with O_2 and NO at temperatures down to 15 K, *J. Chem. Phys.*, *112*, 8466–8469.

Cook, G. R., P. H. Metzger, and M. Ogawa (1965), Photoionization and absorption coefficients of CO in the 600 to 1000 A region, *Can. J. Phys.*, *43*, 1706.

Fahey, D. W., F. C. Fehsenfeld, and E. E. Ferguson (1981), Rate constant for the reaction $C^+ + CO_2$ at collision energies 0.04 to 2.5 eV, *Geophys. Res. Lett.*, *8*, 1115–1117.

Fox, J. L. (1982), Atomic carbon in the atmosphere of Venus, *J. Geophys. Res.*, *87*, 9211–9216.

Fox, J. L. (2003), Effect of H_2 on the Martian ionosphere: Implications for atmospheric evolution, *J. Geophys. Res.*, *108*(A6), 1223, doi:10.1029/2001JA000203.

Fox, J. L. (2004a), Response of the Martian thermosphere/ionosphere to enhanced fluxes of solar soft X rays, *J. Geophys. Res.*, *109*, A11310, doi:10.1029/2004JA010380.

Fox, J. L. (2004b), CO_2^+ dissociative recombination: A source of thermal and non-thermal C on Mars, *J. Geophys. Res.*, *109*, A08306, doi:10.1029/2004JA010514.

Fox, J. L., and F. M. Bakalian (2001), Photochemical escape of atomic carbon from Mars, *J. Geophys. Res.*, *106*, 28,785–28,791.

Fox, J. L., and J. H. Black (1989), Photodissociation of CO in the thermosphere of Venus, *Geophys. Res. Lett.*, *16*, 291.

Fox, J. L., and A. Dalgarno (1979), Ionization, luminosity, and heating of the upper atmosphere of Mars, *J. Geophys. Res.*, *84*, 7315–7333.

Fox, J. L., and A. Dalgarno (1981), Ionization, luminosity, and heating of the upper atmosphere of Venus, *J. Geophys. Res.*, *86*, 629–639.

Fox, J. L., and A. J. Kliore (1997), Ionosphere: Solar activity variations, in *Venus II*, edited by S. Bougher, D. Hunten, and R. Phillips, pp. 161–188, Univ. of Ariz. Press, Tucson.

Fox, J. L., and K. Y. Sung (2001), Solar activity variations in the Venus thermosphere/ionosphere, *J. Geophys. Res.*, *106*, 21,305–21,335.

Fox, J. L., and G. A. Victor (1981), O^{++} in the Venusian ionosphere, *J. Geophys. Res.*, *86*, 2438–2442.

Geoghegan, M., N. G. Adams, and D. Smith (1991), Determination of the electron-ion dissociative recombination coefficient for several molecular-ions at 300 K, *J. Phys. B. At. Mol. Opt. Phys.*, *24*, 2589–2599.

Gougousi, T., M. F. Golde, and R. Johnsen (1997), Electron-ion recombination rate coefficient measurements in a flowing afterglow plasma, *Chem. Phys. Lett.*, *265*, 399–403.

Hedin, A. E., H. B. Niemann, W. T. Kasprzak, and A. Seiff (1983), Global empirical model of the Venus thermosphere, *J. Geophys. Res.*, *88*, 73–83.

Hierl, P. M., R. A. Morris, and A. A. Viggiano (1997), Rate coefficients for the endothermic reactions $C^+ (^2P) + H_2 (D_2) \rightarrow CH^+ (CD^+) + H(D)$ as a function of temperature from 400–1300 K, *J. Phys. Chem.*, *106*, 10,145–10,152.

Hinteregger, H. E., K. Fukui, and B. R. Gibson (1981), Observational, reference and model data on solar EUV, from measurements on AE-E, *Geophys. Res. Lett.*, *8*, 1147–1150.

Howorka, F., A. A. Viggiano, D. L. Albritton, E. E. Ferguson, and F. C. Fehsenfeld (1979), Laboratory studies of O^{++} reactions of ionospheric importance, *J. Geophys. Res.*, *84*, 5941.

Husain, D., and A. N. Young (1975), Kinetic investigation of ground state carbon atoms, C(2^3P_j), *J. Chem. Soc. Faraday. Trans.*, *2*, 71.

Keating, G. M., J. Y. Nicholson, and L. R. Lake (1980), Venus upper atmosphere structure, *J. Geophys. Res.*, *85*, 7941–7956.

Keating, G. M. (1985), Models of the Venus neutral upper atmosphere: Structure and composition, *Adv. Space Res.*, *5*(11), 117–171.

Kimura, M., A. Dalgarno, L. Chantranupong, Y. Li, G. Hirsch, and R. J. Buenker (1993), Rate coefficients for charge transfer of He^+ with C, *Astrophys. J.*, *417*, 812–814.

Knudsen, W. C. (1992), The Venus ionosphere from in situ measurements, in *Venus and Mars: Atmospheres, Ionospheres, and Solar Wind Interactions*, *Geophys. Monogr. Ser.*, vol. 66, edited by J. G. Luhmann, M. Tatrallyay, and R. Pepin, pp. 237–263, AGU, Washington, D. C.

Krasnopolsky, V. A. (1983), Atomic carbon in the atmospheres of Venus and Mars, *Cosmic Res.*, Engl. Transl., *20*, 430–437.

Krasnopolsky, V. A., and V. A. Parshev (1981), Chemical composition of the atmosphere of Venus, *Nature*, *282*, 610–613.

Le Teuff, Y. H., T. J. Millar, and A. J. Marwick (2000), The UMIST database for astrochemistry 1999, *Astron. Astrophys. Suppl. Ser.*, *146*, 157–168.

McElroy, M. B., and J. C. McConnell (1971), Atomic carbon in the atmospheres of Mars and Venus, *J. Geophys. Res.*, *76*, 6674–6690.

Miller, T. M., R. E. Wetterskog, and J. F. Paulson (1984), Temperature dependence of the ion-molecule reactions $N^+ + CO$, $C^+ + NO$, and C^+, CO^+, $CO_2^+ + O_2$ from 90-450K, *J. Chem. Phys.*, *80*, 4922–4925.

Niemann, H. B., W. T. Kasprzak, A. E. Hedin, D. M. Hunten, and N. W. Spencer (1980), Mass spectrometric measurements of the neutral gas composition of the thermosphere and exosphere of Venus, *J. Geophys. Res.*, *85*, 7817–7828.

Nier, A. O., and M. B. McElroy (1976), Structure of the neutral upper atmosphere of Mars: Results from Viking 1 and Viking 2, *Science*, *194*, 1298–1300.

Nier, A. O., and M. B. McElroy (1977), Composition of structure of Mars' upper atmosphere: Results from the neutral mass spectrometers on Viking 1 and 2, *J. Geophys. Res.*, *82*, 4341–4349.

Nier, A. O., W. B. Hanson, A. Seiff, M. B. McElroy, N. W. Spencer, R. J. Duckett, T. C. D. Knight, and W. S. Cook (1976), Composition and structure of the Martian atmosphere: Preliminary results from Viking I, *Science*, *193*, 786–788.

Paxton, L. J. (1983), Atomic carbon in the Venus thermosphere: Observations and theory, Ph.D. thesis, Univ. of Colo., Boulder, Colo.

Paxton, L. J. (1985), Pioneer Venus Orbiter Ultraviolet Spectrometer limb observations: Analysis and interpretation of the 166- and 156-nm data, *J. Geophys. Res.*, *90*, 5089–5096.

Prasad, S. S., and W. T. Huntress (1980), A model for gas phase chemistry in interstellar clouds, I, The basic model, library of chemical reactions, and chemistry among C, N, and O compounds, *Astrophys. J. Suppl.*, *43*, 1.

Rosén, S., R. Peverall, M. Larsson, A. Le Padelled, J. Semaniak, Å Larson, C. Strömholm, W. J. van der Zande, H. Danared, and G. H. Dunn (1998), Absolute cross sections and final state distributions for dissociative recombination and excitation of CO^+ ($v = 0$) using an ion storage ring, *Phys. Res. A.*, *57*, 4462–4471.

Rottman, G. J., and H. W. Moos (1973), The ultraviolet (1200–1900Å) spectrum of Venus, *J. Geophys. Res.*, *78*, 8033.

Scott, G. B. I., D. A. Fairley, C. G. Freeman, M. J. McEwan, and V. J. Anicich (1998), Gas-phase reactions of some positive ions with atomic and molecular nitrogen, *J. Chem. Phys.*, *109*, 9010–9014.

Seiersen, K., A. Al-Khalili, M. J. Jensen, I. B. Nielsen, H. B. Pedersen, C. P. Safvan, and L. H. Andersen (2003), Dissociative recombination of the cation and dication of CO_2, *Phys. Rev. A*, *68*, 022708–022708-6.

Stewart, A. I., D. E. Anderson, L. W. Esposito, and C. A. Barth (1979), Ultraviolet spectroscopy of Venus: Initial results from the Pioneer Venus Orbiter, *Science*, *203*, 777–779.

Taylor, H. A., H. C. Brinton, S. J. Bauer, R. E. Hartle, P. A. Cloutier, and R. E. Daniell (1980), Global observations of the composition and dynamics of the ionosphere of Venus: Implications for the solar wind interaction, *J. Geophys. Res.*, *85*, 7765–7777.

Tobiska, W. K. (2004), SOLAR2000 irradiances for climate change, aeronomy and space system engineering, *Adv. Space. Res.*, *34*, 1736–1746.

Torr, M. R., D. G. Torr, R. A. Ong, and H. E. Hinteregger (1979), Ionization frequencies for major thermospheric constituents as a function of solar cycle 21, *Geophys. Res. Lett.*, *6*, 771–774.

Verner, D. A., and D. G. Yakovlev (1995), Analytic fits for partial photoionization cross sections, *Astron. Astrophys. Suppl. Ser.*, *109*, 125–133.

Woods, T. N., et al. (2000), TIMED solar EUV experiment, *Phys. Chem. Earth C*, *25*, 393–396.

Yung, Y. L., and W. G. DeMore (1982), Photochemistry of the stratosphere of Venus: Implications for atmospheric evolution, *Icarus*, *51*, 199–247.

J. L. Fox, Department of Physics, Wright State University, Dayton, OH 45435, USA. (jane.fox@wright.edu)

L. J. Paxton, Johns Hopkins University Applied Physics Laboratory, 11100 Johns Hopkins Road, Laurel, MD 20723, USA. (larry.paxton@jhuapl.edu)